A Versatile Cell Death Screening Assay Using Dye-Stained Cells and Multivariate Image Analysis

Tony J. Collins,[1,*] Jarkko Ylanko,[2,*] Fei Geng,[3] and David W. Andrews[2]

[1]David Braley Human Stem Cell Screening Facility, Stem Cell and Cancer Research Institute, McMaster University, Hamilton, Ontario, Canada.
[2]Department of Biological Sciences, Sunnybrook Research Institute, Toronto, Ontario, Canada.
[3]School of Engineering Technology, McMaster University, Hamilton, Ontario, Canada.
*These two authors contributed equally to this work.

ABSTRACT

A novel dye-based method for measuring cell death in image-based screens is presented. Unlike conventional high- and medium-throughput cell death assays that measure only one form of cell death accurately, using multivariate analysis of micrographs of cells stained with the inexpensive mix, red dye nonyl acridine orange, and a nuclear stain, it was possible to quantify cell death induced by a variety of different agonists even without a positive control. Surprisingly, using a single known cytotoxic agent as a positive control for training a multivariate classifier allowed accurate quantification of cyto-toxicity for mechanistically unrelated compounds enabling generation of dose–response curves. Comparison with low throughput biochemical methods suggested that cell death was accurately distinguished from cell stress induced by low concentrations of the bioactive compounds Tunicamycin and Brefeldin A. High-throughput image-based format analyses of more than 300 kinase inhibitors correctly identified 11 as cytotoxic with only 1 false positive. The simplicity and robustness of this dye-based assay makes it particularly suited to live cell screening for toxic compounds.

INTRODUCTION

Quantification of cytotoxicity is a common readout for many drug discovery endeavors.[1] Programmed cell death occurs in response to a range of stresses or signals and results from the activation of one or more signaling cascades, including those characteristic of apoptosis, anoikis, necrosis, necroptosis, and autophagic cell death, and the limitations of the various current assays have been recently reviewed.[2,3] Furthermore, death is generally cell autonomous and results in loss of cell adhesion complicating image-based assays of adherent cells. Detachment from the growth support or neighboring cells is not only a cell death response but also leads to cell death through anoikis; therefore, flow-based methods can overestimate cytotoxicity.

While many assays have been developed to quantify specific aspects of cell death, it has been suggested that to detect the broad spectrum of cell death cascades with high sensitivity, measurements of multiple relatively early indicators should be integrated.[3] Such an approach is generally impractical for high-content screening because of the cost and time associated with multiple often incompatible assays. Most techniques for image-based analysis of the effects of small-molecule compounds use techniques such as immunostaining that are expensive, require extensive optimization, and are incompatible with living cells,[4] or multiple dyes necessitating fixation and multiple processing steps (typically 5–10 steps in commercial kits).[5]

We propose an alternative image-based cytotoxicity assay for adherent cells that integrates measurement of organelle ultrastructural changes and alterations in mitochondrial function associated with programmed cell death. Unlike many cell death assays, this method uses only two dyes that can be added to cells together without a washing step, requires minimal handling or optimization, and is easily analyzed using multivariate methods available in multiple commercial

and open-source software packages to enable quantification of single cells. Multivariate image analysis algorithms attempt to integrate as much of the information of each cell that can be extracted. This approach takes a broad variety of measurements (referred to as "features") from each cell to obtain a "feature-fingerprint." These are then compared to reference "feature-fingerprints," and each cell is classified to the closest matching reference dataset. Using these techniques, subcellular localization of proteins,[6,7] cellular subpopulations,[8] and drug mechanism of action[4,5,9] have been correctly classified with often greater than 95% accuracy.

In this study, we describe a simple approach to quantify cytotoxicity in adherent cells based on multivariate analysis of cells stained with the inexpensive dye, nonyl acridine orange (NAO), and a nuclear stain (MVA-NAO). NAO is a lipophilic cationic dye with some preference for binding cardiolipin and has been shown to also be partially sensitive to the mitochondrial membrane potential.[10] We compare MVA-NAO classification with more traditional measures of apoptosis and find that it provides improved classification in screening, quantified as improved Z′ factor (Z′), a standard screening assay metric. Moreover, this dye combination can be used to quantify EC_{50} values when used in a dose–response format. With an average cost that ranges from \$0.1–10 per plate (depending on the nuclear stain), compared to commercial kits that average \$50 per plate, this method is particularly well suited for applications involving large numbers of samples, such as high-content screening.

MATERIALS AND METHODS

Cell Culture and Reagents

Human breast cancer cells MCF-7 were maintained in the α-minimal essential medium (α-MEM; Life Technologies, Carlsbad, CA) supplemented with 10% fetal bovine serum (HyClone, Logan, UT). Cells were seeded, treated, and stained under Biosafety level 2 conditions using a custom Sample Preparation WorkCell platform (Thermo Fisher CRS, Burlington, ON, Canada) that contains a CRS VAL 3-axis robot (Thermo Fisher) for plate handling, Combi Multidrop dispensers (Thermo Fisher), ELx plate washers (Biotek, Winooski, VT), and a STARlet 96-tip robot (Hamilton, Reno, NV) for precise liquid dispensing. Cells were seeded at a cell density of 5,000 cells per well to a 384-well plate (Cell Carrier; PerkinElmer, Waltham, MA) and grown for 24 h before drug treatment, or transfected with a plasmid encoding the caspase sensor (a kind donation from Dr. R. Truant, McMaster University) using NanoFect (QIAGEN, Venlo, Limburg, Netherlands) reagent according to the manufacturer's standard protocol, 24 h before drug treatment.

Drug Treatments

Drugs were dissolved in (DMSO; Bioshop, Burlington, ON, Canada) and diluted to the final assay concentrations in α-MEM. Tumor necrosis factor-alpha (TNFα), cycloheximide, thapsigargin (TG), brefeldin A (BFA), dithiothreitol (DTT), actinomycin D, staurosporine, tamoxifen, and tunicamycin, were purchased from Sigma-Aldrich (St. Louis, MO). The panel of 320 kinase inhibitors was obtained from the Ontario Institute for Cancer Research.

Cell Staining

Cells were incubated under culture conditions with fluorescent dyes for 30 min before image acquisition, using either 100 nM NAO (Sigma-Aldrich) or 10 nM tetramethylrhodamine, ethyl ester (TMRE; Life Technologies) in α-MEM, or 1 μM propidium iodide (PI; Sigma-Aldrich) and 1:100 Annexin V Alexa Fluor 488 (Life Technologies) in 0.01 M HEPES pH 7.4, 0.14 M NaCl, and 2.5 mM $CaCl_2$. For the experiments reported here we used 5 μM DRAQ5 (Biostatus, Leicestershire, UK) as a nuclear dye for cell identification and segmentation; however, we have successfully used other nuclear dyes, including Hoescht and DAPI for this purpose.

Biochemical Assays

For analysis of poly ADP-ribose polymerase (PARP) cleavage, light chain 3 (LC3), and glucose-regulated protein (Grp) 78 and Grp94 levels, proteins were separated on 8% denaturing sodium dodecyl sulfate–polyacrylamide gel electrophoresis (SDS-PAGE) gels and transferred to polyvinyl difluoride membrane, incubated with a 1:1,000 dilution of PARP C-2–10 monoclonal antibody or KDEL antibody to detect Grp78 and Grp94 from Enzo Life Sciences (Farmingdale, NY), LC3 antibody from Cell Signaling Technologies (Danvers, MA), and the antibody to actin used for normalization was from Santa Cruz Biotechnology (Dallas, TX). These antibodies were detected with a 1:10,000 dilution of the corresponding horseradish peroxidase-conjugated secondary antibody from Jackson ImmunoResearch Laboratories (West Grove, PA), and Enhanced Chemiluminescence reagents (EMD Millipore, Billerica, MA) and band intensities were recorded using a CCD camera-based imager (MicroChemi 4.2; FroggaBio, Toronto, ON, Canada). Where required, band intensities were corrected for unequal loading by reprobing the blots for actin.

Microscopy

All cells were imaged at 37°C and 5% CO_2 using an Opera QEHS high-content screening system (PerkinElmer) with environmental control for the imaging chamber and a tunable Ti:Sapphire pulsed laser and frequency doubler from Coherent

(Santa Clara, CA). Images were acquired using 40×0.9 NA and 20×0.7 NA water immersion objectives. Data shown were recorded with the 40× lens, however, similar results were obtained with either lens. Images of NAO and Annexin V Alexa Fluor 488 staining were acquired with 488 nm excitation and 520/35 emission filter; PI and TMRE with 561 nm excitation and 600/40 emission; DRAQ5 with 633 nm excitation and 690/50 nm emission. Because the fluorescence intensity of NAO is as high as most nuclear stains, it is possible to image 384-well plates rapidly. Generally, for imaging multiple fields of view per well (here 3–8), the time depends primarily on the instrument used and typically ranges from 15 to 30 min. Fluorescence images of monomeric Cerulean (mCer) in the caspase sensor were collected with 430 nm nanosecond pulsed excitation and 475/50 emission, using a fast gated CCD camera. For ratiometric Förster resonance energy transfer (FRET), mCer was excited as above and fluorescence was recorded from the Venus fluorescence protein using the 520/35 emission filter.

Image and Data Analysis

Images collected on the Opera were analyzed using Acapella 2.5 (PerkinElmer). Assay-specific features of fluorescence intensity and texture features, including Haralick texture[10] features and threshold adjacency statistics,[6] were calculated using custom algorithms (scripts available from www.andrewslab.ca). Similar methods are available in commercial software packages, including Acapella, Harmony, and Columbus, and in open source programs such as CellProfiler and OME. We have found that multiple software packages perform equally well with the images analyzed here. Cell masks were identified from DRAQ5 images with Acapella routines that perform similar to those in CellProfiler. A full list of the 235 features used is available from the authors. Values for each cell were generated and exported to MATLAB for further analysis.

In MATLAB, the cell-level data were transformed to z-scores and well averages calculated for each feature. Support vector machine (SVM) classifiers were trained (MATLAB function *svmtrain*()) using well-level data and then used to classify cell-level data (*svmclassify*()). The fraction of individual cells per well per classified group was calculated. Various measures of cell death were compared by Z-factor analysis, using the mean and standard deviation of eight untreated negative control and four TNFα-treated positive control replicate wells per assay.

RESULTS

MVA-NAO of Images of Dye-Stained Cells Is More Sensitive and More Robust than Standard Fluorescence Imaging Methods for Measuring Cell Death

Several conventional image-based assays used to quantify cell death are illustrated for MCF-7 breast cancer cells 24 h post-treatment with TNFα and cycloheximide (referred to here as TNFα treatment), a standard method for inducing extrinsic apoptosis (*Fig. 1*). Annexin V binding measures the externalization of phosphatidylserine that occurs during apoptosis
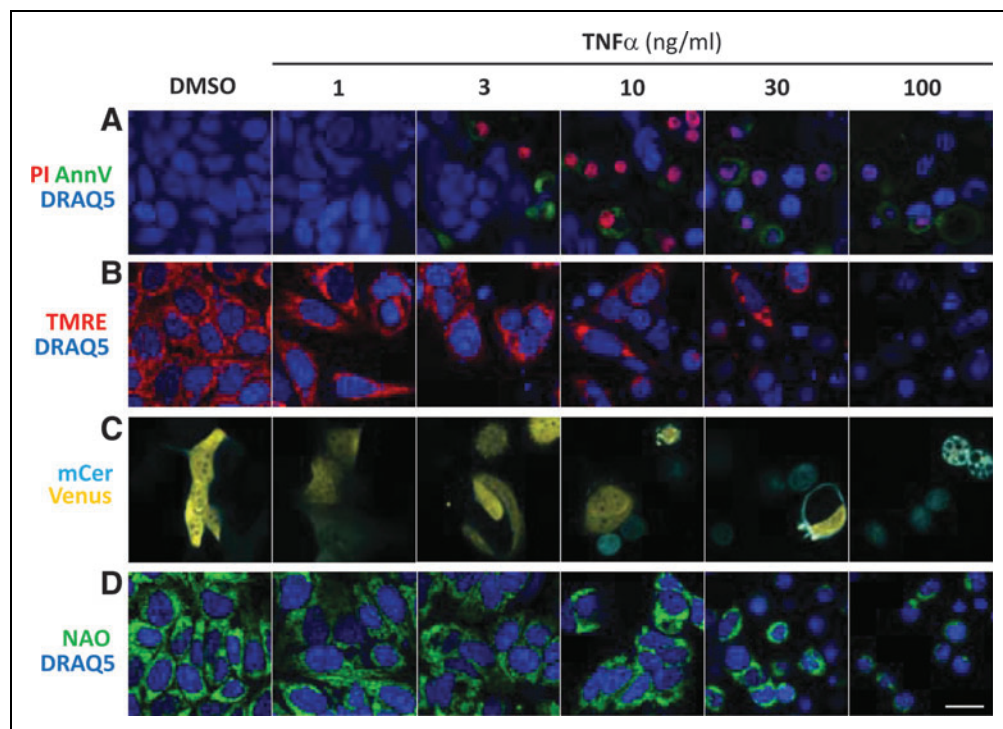

Fig. 1. Image-based cell death assays. Example images of cells 24 h after TNFα treatment by the fluorescence assays under evaluation. For each assay, the relevant channels were merged, pseudocolored, and adjusted for brightness and contrast. **(A)** Cells stained with propidium iodide (PI, *red*), Annexin V Alexa Fluor 488 (AnnV, *green*), and DRAQ5 (*blue*). **(B)** Cells stained with tetramethylrhodamine, ethyl ester (TMRE; *red*), and DRAQ5 (*blue*). **(C)** Intensity weighted ratio images of cells expressing the caspase sensor showing monomeric Cerulean (mCer; *cyan*) and stimulated emission of Venus (Venus, *yellow*). **(D)** Cells stained with nonyl acridine orange (NAO; *green*) and DRAQ5 (*blue*). Scale bar = 20 μm.

when cells no longer retain the plasma membrane lipid asymmetry. However, as seen from the images in *Figure 1*, Annexin V binding was useful for a limited number of TNFα treatments, because at higher doses staining decreases as cells fragment and die. PI staining measures the loss in integrity of the plasma membrane that occurs early in necrosis, but late during apoptosis, but also has a narrow detection range (*Fig. 1A*). TMRE, a cell-permeant, cationic, red-orange fluorescent dye sequestered by active mitochondria and used to quantify mitochondrial membrane potential, has an intermediate detection range (*Fig. 1B*).

Caspase activation, a hallmark of apoptosis, was measured using a Cerulean and Venus fluorescence protein FRET-based caspase reporter (*Fig. 1C*). Cleavage of the sensor at the caspase 3/7 site DEVD separates the donor (mCer) from the acceptor yellow fluorescence protein (Venus) abolishing FRET and decreasing the fluorescence of the acceptor. This assay reliably detects apoptosis, but no other forms of cell death, and requires the cells be transfected to express the sensor. Nuclear condensation and cell counts were derived from DRAQ5 staining in cells (*Figs. 1A, B, D,* and *2B*).

In contrast to these conventional assays, NAO stains multiple subcellular membrane structures, emphasizing the mitochondria due to their high membrane potential and cardiolipin content and reports on cell death indirectly (*Fig. 1D*). Under these conditions, changes in cell ultrastructure characteristic of cell death due to TNFα are visually obvious, and the assay has a large detection range and requires minimal optimization.

For the conventional image-based assays, response to drug treatment was detected on a cell by cell basis by segmenting the micrographs using the DRAQ5 image and applying an intensity threshold established from the untreated samples to the other channel. As little as 10 ng/mL TNFα treatment was detected by all of these assays (*Fig. 2*). Annexin V staining was the most sensitive and allowed detection ($P < 0.005$) at 0.3 ng/mL, very similar to biochemical analyses that detected caspase-dependent cleavage of PARP to the characteristic cleaved form (ΔPARP), in response to treatment with 1.0 ng/mL TNFα (*Fig. 2F, G*). The biochemical assays provide a wealth of information that is unfortunately convolved, including increased total PARP in response to DNA damage or stress,
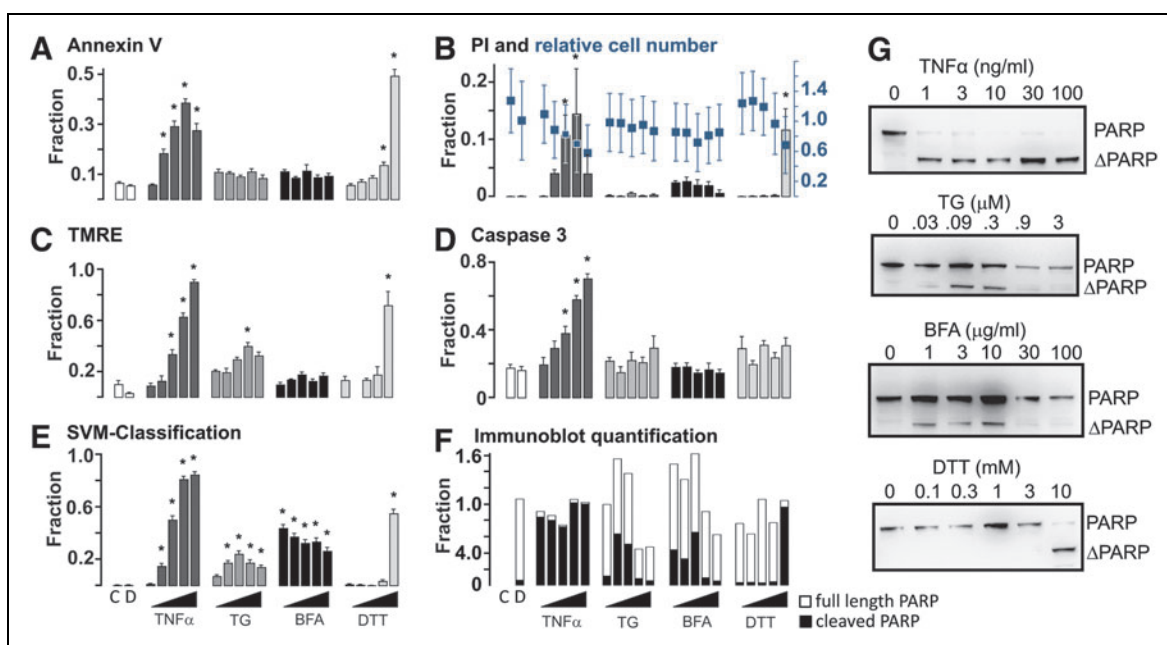

Fig. 2. Cell death measurements using conventional image-based assays are not as sensitive as MVA-NAO and immunoblotting. **(A–F)** Histograms illustrating the response of cells to the negative control **(C)** with no addition, dimethylsulfoxide (DMSO), or TNFα (1, 3, 10, 30, 100 ng/mL), thapsigargin (TG; 30, 90, 300, 900 nM, 3 μM), brefeldin A (BFA; 1, 3, 10, 30, 100 μg/mL), and dithiothreitol (DTT; .1, .3, 1, 3, 10 mM) measured using the indicated assay. The fraction of cells scored as affected using an arbitrary threshold for conventional image-based methods of quantifying apoptosis, including **(A)** Annexin V, **(B)** PI and cell number (*blue*), **(C)** TMRE, and **(D)** caspase activity compared to **(E)** MVA-NAO for a range of proapoptotic treatments. Bars indicated with * were significantly different than the negative controls (*t*-test, $P < 0.05$, $n = 4$). **(F–G)** Immunoblots for poly-ADP ribose polymerase (PARP) indicate apoptosis as cleavage of PARP to ΔPARP (migration positions indicated to the *right* of the blots) or necrosis as degradation of PARP (loss of both bands), **(F)** quantified after correction for actin levels measured from the same blots.

cleaved PARP due to apoptosis, and degraded PARP due to necrosis.[11] As expected, TNFα treatment induced only apoptosis while most of the other drugs elicited stress, necrosis, and apoptosis. As a result, the correlation of the blotting results and the high-content methods requires close examination of the quantified data.

The fraction of Annexin V-positive cells peaked at 40% for TNFα treatment and decreased at higher doses due to loss of staining of the cells (*Fig. 1*). Other assays suggest this is an underestimate of cells undergoing cell death as caspase activation, and TMRE staining identified 70%–90% of cells as having responded to TNFα treatment (*Fig. 2C, D*). Interestingly, the highest concentration of TNFα, shown by other measures to produce the highest level of cell death, results in a low measure of death as quantified by PI (*Fig. 2B*). As shown in *Figure 1*, at the latter stages of cell death there is sufficient DNA degradation to reduce PI staining leading to false negatives. Furthermore, cell count based on DRAQ5 staining was highly variable and at our assay time point was for most treatments relatively unchanged, thus limiting its usefulness to detect cell death (*Fig. 2B*).

Conventional image-based assays were not sensitive for detecting changes in cells induced by TG, an endoplasmic reticulum calcium pump inhibitor, BFA, a toxin that blocks forward vesicular transport between the endoplasmic reticulum and Golgi, or DTT, a reducing agent that causes protein misfolding in the endoplasmic reticulum by preventing proper disulfide bond formation. Concentrations of 0.09 μM TG and to a limited extent 1–10 μg/mL BFA were found to induce PARP cleavage 24 h post-treatment in immunoblot-based assays. However, cellular responses, as assessed by PARP immunoblots, are complicated for TG and BFA as the drug induced damage results in increased PARP levels in cells, while apoptosis caused PARP to be cleaved at a site specific for caspases 3 and 7, and necrosis results in degradation of both PARP bands (*Fig. 2F, G*) as seen previously for other drug treatments.[11]

After 0.9 μM treatment with TG, a small but statistically significant response was detected using TMRE. A response to BFA treatment was not detected for any concentration using any of the conventional image-based readouts of cell death (*Fig. 2A–D*). These results demonstrate that conventional image-based assays fail due to the limited range of drug treatments they respond to and inaccurate scoring of cells undergoing nonapoptotic responses to drugs such as TG and BFA.

Only the highest concentration of DTT (10 mM) showed significant change in PI positivity, TMRE negativity, and Annexin V staining. The latter was significantly different ($P < 0.01$) between control and 3 mM DTT. Consistent with this

result and expectation based on the known propensity of DTT to cause cell stress that only leads to the unfolded protein response triggering apoptosis in extreme conditions, 10 mM DTT was also required to induce apoptosis detected biochemically (*Fig. 2G*). Caspase 3 positivity reliably detected only TNFα treatment (*Fig. 2D*) and death due to the highest concentration of DTT. This may be because activation of caspase 3 is a response to apoptosis and the PARP western blots reveal minimal PARP cleavage in response to TG or BFA. Instead, PARP degradation characteristic of necrosis[2] is seen at the higher concentrations of these drugs (*Fig. 2F, G*).

To improve the detection of cytotoxicity due to all of these agents, we used MVA-NAO. Images were acquired (*Table 1*), and the DRAQ5 images were used to identify the cell nuclei and cytoplasmic masks. These masks were then used to quantify 235 features for each cell from the NAO and DRAQ5 images. These features included texture, intensity, shape, and size descriptors for the cytoplasm and nuclei.

A simple threshold cannot be used with multiparametric data; therefore, to process the features from NAO- and DRAQ5-stained cells, we used classification with a SVM, a standard multivariate approach (*Fig. 2E*). An SVM was generated that maximally classified random subsets of the control cells as either negative (untreated) or positive (treated), based on images of the cells either untreated or exposed to 100 ng/mL TNFα, respectively. Traditionally, an SVM is calculated based on a positive and negative control for each treatment. However, to mimic screening data, the images from TNFα-treated and vehicle-treated wells were used as high and low controls to train a classifier that was then applied to all of the drug treatments. The fraction of cells classified as positive (number of positive cells/well divided by the total number of cells/well) was then expressed for each well as a measure of cytotoxicity.

MVA-NAO showed significant differences in the fraction of cells classified positively between control and 3 ng/mL TNFα treatment, the lowest TNFα concentration detected by conventional image-based approaches (compare *Fig. 2A–D* with *E*). SVM classification resulted in a similar high fraction response for TNFα treatment as seen with TMRE and caspase activity (~0.8). However, unlike the conventional methods, multivariate analysis detected responses to all concentrations of BFA and to all but the lowest concentration of TG. Biochemical assays, in which caspase mediated cleavage and degradation of PARP, were used to assess apoptosis and necrotic cell death, respectively, and to detect only population averages not individual cells. Nevertheless, inspection of the immunoblots used to assess PARP cleavage and degradation suggests that the biochemical data are qualitatively most

Table 1. MVA–NAO Screening Protocol			
Step	**Parameter**	**Value**	**Description**
1	Plate cells	40 μL	5,000 cells/well
2	Incubation time	18–24 h	37°C, 5% CO_2
3	Controls	10 μL	Diluted in HEPES, added at final 1× concentration
4	Library compounds	10 μL	Diluted in HEPES, added at final concentration of 1 uM
5	Incubation time	24 h	37°C, 5% CO_2
6	Dye addition	50 μL	Diluted in media, added at final concentrations of 100 nM NAO, 5 uM DRAQ5
7	Incubation time	1 h	37°C, 5% CO_2
8	Assay readout	Excitations at 488 and 635 nm, emissions at 520 and 690 nm	Opera QEHS
9	Multivariate feature extraction	n Features	Descriptors of texture, shape, and size per cell; $n = 235$
10	Feature scaling	z-Score	For each descriptor, feature mean scaled to 0, and standard deviation set as whole number increments from mean
11	SVM classification		
(a)	Classifier training	n Features on m high and low control wells	Well-level averages for all features in DMSO (low control) and TNFα+CHx (high control) wells; $m = 32$
(b)	Cell-level classification	n Features of k query cells	$k > 400$ per query well
12	Euclidean distance analysis		
(a)	Control centroid calculation	Well means of n features of m low control wells	Calculate centroid of DMSO well means; $m = 16$
(b)	Distance measure	Well means of n features of m query wells	Distance of query well mean of DMSO centroid; $m = 320$

Step Notes
1. Cells dispensed at all wells of a black wall clear-bottom cell culture plate.
3. Added to columns 1, 2, 23, and 24.
4. Added to columns 3–22.
8. Imaging performed at constant 37°C, 5% CO_2.
9. A completed list of measured features is available from the authors on request.
10. Performed if positive and negative experimental controls are present.
12. Performed if only negative experimental control is present.
DMSO, dimethylsulfoxide; NAO, nonyl acridine orange; SVM, support vector machine; TNFα, tumor necrosis factor-alpha.

similar to the results obtained using multivariate analysis of images of cells stained with NAO and DRAQ5 (*Fig. 2E, F*), consistent with these techniques being superior to other image-based techniques. For both TG and BFA, MVA-NAO was less sensitive at the two highest drug concentrations where the biochemical assays suggested there was significant cell death due to necrosis (degradation of both PARP bands). In contrast, the PARP immunoblots for cells treated with TNFα show evidence only of apoptosis (cleavage of full-length

PARP to ΔPARP). Since images of cells treated with TNFα were used as the training group, the absence of necrosis in the positive control may explain why the classifier was less sensitive for images of cells undergoing necrosis (*Fig. 2E* compared to *F*).

To compare the different methods quantitatively, Z′-values were calculated for a range of conventional measures of cell death, including those shown in *Figure 2A–D* and MVA-NAO. The highest performing conventional assay was TMRE with a

Table 2. Z' Calculated from Untreated and 100 ng/mL TNFα Treatments	
Apoptosis	Z'
NAO-SVM	0.91
TMRE positive	0.57
Caspase-3 activity	0.34
Annexin V positive	0.01
Cell count	−0.3
NAO intensity	−1.38
PI positive	−4.0
Nuclear area	−27

PI, propidium iodide; TMRE, tetramethylrhodamine ethyl ester.

Z' of 0.57. Other measures such as cell count, nuclear condensation (i.e., nuclear area), and loss of membrane integrity (PI positivity) were poor screening assays with Z' of less than zero in this assay format (Table 2). To derive a Z' value for MVA-NAO, we used the readily interpretable "percentage of cells per well classified as positive." The resulting Z' value of 0.91 outperformed all of the conventional image-based cell death assays (Table 2).

Derivation of Dose–Response Curves Using MVA–NAO

Secondary assays in screening campaigns often aim to derive the EC_{50} concentration of active compounds based on their dose-dependent effects on cells. To further test the utility of MVA-NAO for high-content screening, cells were treated with a range of concentrations of compounds chosen to target a variety of cell death or stress pathways. As above, the extrinsic apoptosis pathway was targeted by TNFα treatment. In addition, drugs were added to cause endoplasmic reticulum stress (tunicamycin); intrinsic apoptosis (staurosporine),[12] autophagy (low-dose tamoxifen), and mitotic catastrophe (actinomycin D)[13] (Fig. 3A) and the percentage of cells classified positive for each treatment were quantified. Unlike the experiments described above in which we used images of only TNFα-treated cells as the positive controls, here we used the highest concentration of each treatment as its respective positive training set and derived EC_{50} values for the response (Fig. 3B). Using this approach, it was possible to generate dose–response curves for each of the cell treatments.

The dose–response curves for the drugs that induce apoptosis (TNFα, actinomycin D and staurosporine) exhibit the expected S-shape curves with EC_{50}s of 5 ng/mL, 60 nM, and 125 μM, respectively, and these drugs show similar dose-dependent apoptosis as assessed by the cleavage of PARP (Fig. 3C). Moreover, both actinomycin and staurosporine exhibit a marked transition in PARP cleavage at a drug concentration near the EC_{50} determined by NAO-MVA.

As expected, the PARP cleavage does not correlate nearly as well with the dose–response curves obtained by MVA-NAO for tamoxifen and tunicamycin, drugs that cause autophagy and endoplasmic reticulum stress, respectively. Biochemical assessment of autophagy for tamoxifen-treated cells by immunoblotting for activated LC3 permits detection of autophagy at 5 μM and shows a sharp increase between 9.4 and 18 μM. Cleavage of PARP indicative of apoptosis is not detected for tamoxifen-treated cells, but degradation is pronounced by 5 μM. MVA-NAO was less sensitive and detects a sharp transition in phenotype at around 60–70 μM tamoxifen. For tunicamycin, biochemical detection of endoplasmic reticulum stress as increased levels of Grp78 and Grp94 is apparent at 0.8 μM. In contrast, MVA-NAO does not detect phenotypic changes in tunicamycin-treated cells until around 10 μM with an EC_{50} that can only be estimated in the absence of saturation of almost 80 μM. These results for tamoxifen and tunicamycin are consistent with MVA-NAO trained on the highest dose of the drugs detecting common features of dying cells and, therefore, being less sensitive at detecting changes due to autophagy or endoplasmic reticulum stress.

While MVA-NAO enabled comparing cell death induced by different concentrations of a single treatment, in most screens the effect of unknown compounds is compared to a single positive control. To mimic this situation, images of cells treated with the highest concentration of TNFα and stained with NAO and DRAQ5 were used to train an SVM, as above, which was then applied to all of the other sets of images. In this situation, the different doses of the various compounds act as surrogates for compounds with different activities. The resulting dose–response curves were surprisingly similar to those generated using a separate SVM for each drug treatment (Fig. 3D), suggesting that MVA-NAO can be used in a screening format to examine a variety of drugs suffering only a small loss in sensitivity compared to an optimized assay.

MVA–NAO Identification of Cytotoxic Kinase Inhibitors

The data above strongly suggest that MVA-NAO can be used to identify toxic compounds in libraries of small molecules. To test this directly, an annotated small-molecule kinase inhibitor library was assayed at 1 μM with TNFα (at
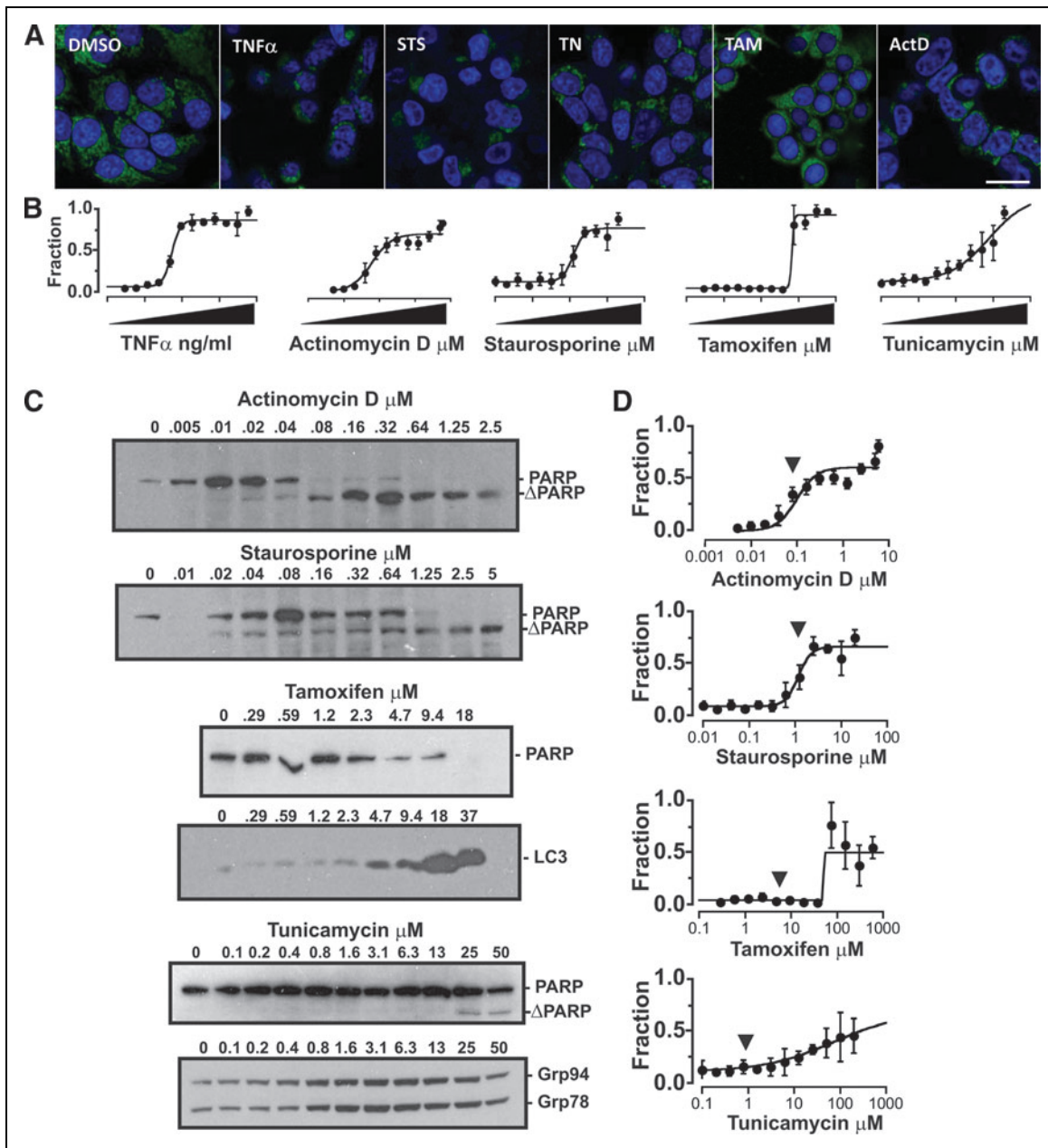
Fig. 3. Cell death dose–response curves generated for cytotoxic compounds by MVA-NAO are comparable to those obtained by immunoblotting. **(A)** Example images of cells 24 h after drug treatment. Merged, pseudocolored images of NAO (*green*) and DRAQ5 (*blue*) were adjusted for brightness and contrast. Panels show cells with no treatment (DMSO) or with 150 ng/mL TNFα, 5 μM STS, 50 μM TN, 150 μM TAM, and 2.5 μM ActD. Scale bar = 20 μm. **(B)** Dose–response curves generated by MVA-NAO for TNFα (0.2–500 ng/mL), the cytotoxic drugs actinomycin D and staurosporine, and agents that cause autophagy (tamoxifen) or endoplasmic reticulum stress (tunicamycin). Increasing dose is indicated by the *triangle*, range is indicated in **(D)**. Images of cells treated with DMSO and the highest dose of each drug were used to generate a classifier for that drug. Each point represents the average and standard deviation in fraction of cells/well classified as affected by the drug of eight replicate wells. **(C)** Detection of cell death, autophagy, and endoplasmic reticulum stress by immunoblotting cell lysates for PARP, light chain 3 (LC3), glucose regulated protein (Grp) 94, and Grp78 (bands are indicated to the *right* of the blots). Cleavage of PARP to ΔPARP indicates apoptosis, while degradation of PARP and ΔPARP indicates necrosis. Detection of the activated (cleaved and lipidated) form of LC3 indicates autophagy. Increased amounts of the abundant KDEL containing proteins Grp94 and Grp78 indicate endoplasmic reticulum stress. **(D)** Dose–response curves generated by MVA-NAO for the indicated drugs. Images randomly selected from the DMSO control and the highest dose TNFα were used to generate a classifier that was applied to images obtained for cells treated with the other drugs. Each point represents the average and standard deviation in fraction of cells/well classified as affected by the drug of eight wells. The downward *arrow* indicates the dose at which a change in phenotype was detected by immunoblotting.

29 ng/mL based on *Fig. 3A*) and 0.1% DMSO as high and low controls, respectively. At 1 μM, most of the kinase inhibitors in the library are not expected to be toxic. Afterward, drug treatment cells were stained with NAO and DRAQ5 as above. To validate the assay for high-throughput-type experiments, where image acquisition is often the rate-limiting step, we reduced the magnification used to 20× and the numbers of fields acquired to 3. At this magnification and resolution, the Z′ was still high (Z′ = 0.62) and throughput was much increased (a 384-well plate could be imaged in less than 30 min).

A heat map for the results illustrates the fraction of cells in each well scored as similar to the positive control (*Fig. 4*). Based on compound annotation for other cell lines (*Table 3*), we defined as toxic compounds in which more than 50% of the cells scored similar to TNFα. To confirm that this was a sufficiently stringent arbitrary criterion to identify toxic compounds, we treated cells with 1 μM of the 11 kinase inhibitors that scored positive as above and then assessed 6 days after treatment whether cells exposed to these compounds were still viable. With the exception of Dasatinib, all of the cells treated with the compounds designated as toxic by MVA-NAO eventually died (data not shown). This result confirms that MVA-NAO can be used to identify toxic compounds in a screening-type assay.

DISCUSSION

A cell is considered dead *in vitro* when it loses plasma membrane integrity[2,3]; however, a cell can be committed to dying long before this point is reached. Initiation of cell death processes is associated with a wide range of measurable changes within the cell.[2] Biochemical assays based on
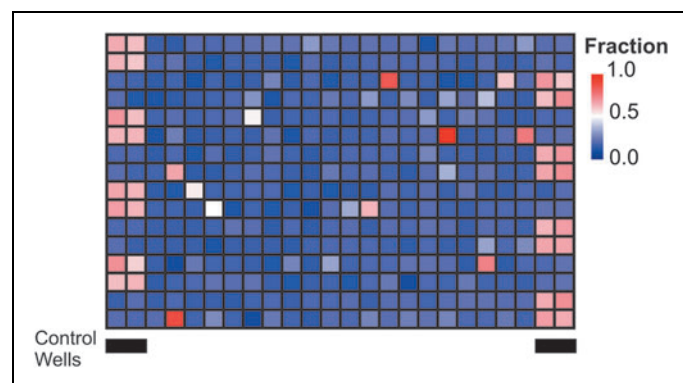
Table 3. Cytotoxicity of Kinase Inhibitors				
Compound	Targets	Fraction	Relevance	Reference
Alvocidib/ Flavopiridol	CDK	0.98	Chronic lymphocytic leukemia	18
SNS-032	CDK	0.88	Chronic lymphocytic leukemia	19
PIK-75	PI3K	0.86	Acute myeloid leukemia	20
GSK-461364	PLK1, PLK3	0.76	Solid tumors	21
BI 2536	PLK1	0.75	Solid tumors	22
Volasertib	PLK1	0.66	Solid tumors	23
BMS-3	LIMK	0.63	Unknown	N/A
JNJ-10198409	PDGFR	0.6	Glioblastoma	24
Staurosporine	Pan kinases	0.54	Pan kinase inhibitor	25
Dasatinib	bcr-Abl, Src	0.52	Chronic myeloid leukemia	26
AZ-960	JAKs	0.51	Adult T-cell leukemia	27

immunoblotting permit such determinations for averaged cell populations, but are labor intensive and slow. While image-based techniques are amenable to a high-throughput report on individual cells and can report statistically significant changes, currently available image-based techniques require multiple steps, optimization, and are expensive, making them suboptimal for a drug screen aimed at providing biochemical-quality data (*Fig. 2*).

For a screen, the assay needs to be able to identify compounds as either active or inactive based on data from one sample (*i.e.*, well), so any overlap in the distribution of response between active and inactive treatments results in false readouts. Moreover, the mechanism of cell death by any one compound may be very different than the positive control used in the screen. Ideally, the assay should not score stress responses as cytotoxic unless the stress is so acute that the cells will eventually die. Our results suggest that MVA-NAO fulfills all of these criteria as the dye is inexpensive, requires only a single addition step, no wash, and relatively little optimization. Due to the excitation sources available, we chose DRAQ5 as the DNA stain. Similar results would be obtained with a UV-based DNA stain (DAPI or Hoechst) on instruments capable of UV excitation, making this approach broadly applicable. Furthermore, the multivariate techniques needed to interpret the image data are commonly included in image processing software packages.

Fig. 4. Cytotoxic kinase inhibitors identified by MVA-NAO screening. MVA-NAO heat map where the *color* indicates the fraction of cells per well classified as affected (similar to TNFα treated), as indicated to the *right* of the panel. Columns of control wells containing cells treated with either TNFα or DMSO (*pink* or *blue*, respectively) are indicated below the panel.

The quality of a screening assay is typically measured through calculation of a Z′ value based on high and low control treatments.[14,15] In our hands, 24 h post-treatment, traditional measures of apoptosis such as cell count, nuclear shrinkage, and Annexin V staining all showed highly significant changes between our low controls (untreated) and high controls (TNFα), but low Z′ values (*Table 2*). Other measures gave better Z′ values, such as measures of mitochondrial membrane potential and caspase activation, but the highest Z′ values were obtained using MVA-NAO. As well as giving improved Z′ values for TNFα as a high control, MVA-NAO was able to identify toxicity induced by TG and BFA—known activators of cell death—at concentrations much lower than was detected by other image-based apoptosis assays (*Fig. 2*). In fact, only MVA-NAO detected activity in BFA at concentrations found to induce PARP cleavage in immunoblot.

In multivariate image analysis, a classifier is trained using features from cells known to be from the two classes to be separated. Selection of data for each class for training can be data from individual cells that a user has manually selected and identified[16] or from a random subset taken from cells treated with or without known modulators of the response under study. Screening experiments are typically designed with in-plate controls, which inherently lend themselves to use as training data. In our case, we used the in-plate controls as training sets to remove the laborious manual classification step. Furthermore, to remove concerns about outlier cells affecting the reproducibility of the classifier when making random selections, we have taken a pragmatic approach using population averages from the high and low control wells as positive and negative controls, respectively, to train the classifier. This also simplifies and expedites the training of the classifier. While we used well-level averages to train the classifier, we used cell-level data, not well-level averages, for classification of unknown compounds. Using well-level averages would have resulted in a binary decision for the well and not have allowed sufficient granularity for ranking activity or derivation of dose–response curves.

Surprisingly, we found that a single activator of apoptosis (TNFα) could be used to correctly, although with reduced sensitivity compared to the appropriate biochemical assay, classify activators of other cell death pathways. Comparison of the MVA-NAO data with the results of biochemical analyses for apoptosis, necrosis, endoplasmic reticulum stress, and autophagy suggests that when the classifier is trained on a positive control that kills cells exclusively by apoptosis, it is less sensitive at detecting cells dying by necrosis and does not incorrectly score endoplasmic reticulum stress or autophagy as cytotoxic unless the drug concentration is sufficiently high to kill cells. This is supported by the dose–response curve for tunicamycin, which does not plateau over the concentrations we have tested here.

Many drug trial failures and withdrawals can be attributed to unexpected organ toxicity. As such, predictive toxicity assays play a key role in drug development. Many idiosyncratic drug toxicities are correlated with mitochondrial function. Since NAO-related features will be correlated to mitochondrial function and structure, this assay should be useful for early identification of drug toxicity.[17]

ACKNOWLEDGMENT

DISCLOSURE STATEMENT
No competing financial interests exist.

REFERENCES

1. Galluzzi L, Bravo-San Pedro JM, Vitale I, *et al.*: Essential versus accessory aspects of cell death: recommendations of the NCCD 2015. *Cell Death Differ* 2015;22:58–73.

2. Kepp O, Galluzzi L, Lipinski M, Yuan J, Kroemer G: Cell death assays for drug discovery. *Nat Rev Drug Discov* 2011;10:221–237.

3. Klionsky DJ, Abdalla FC, Abeliovich H, *et al.*: Guidelines for the use and interpretation of assays for monitoring autophagy. *Autophagy* 2012;8:445–544.

4. Caie PD, Walls RE, Ingleston-Orme A, *et al.*: High-content phenotypic profiling of drug response signatures across distinct cancer cells. *Mol Cancer Ther* 2010;9:1913–1926.

5. Gustafsdottir SM, Ljosa V, Sokolnicki KL, *et al.*: Multiplex cytological profiling assay to measure diverse cellular states. *PLoS One* 2013;8:e80999.

6. Hamilton N, Pantelic R, Hanson K, Teasdale R: Fast automated cell phenotype image classification. *BMC Bioinformatics* 2007;8:110.

7. Murphy R, Velliste M, Porreca G: Robust numerical features for description and classification of subcellular location patterns in fluorescence microscope images. *J Signal Process Syst.* 2003;35:311–321.

8. Loo L-H, Lin H-J, Steininger RJ, Wang Y, Wu LF, Altschuler SJ: On an approach for extensibly profiling the molecular states of cellular subpopulations. *Nat Methods* 2009;6:759.

9. Loo L-H, Wu LF, Altschuler SJ: Image-based multivariate profiling of drug responses from single cells. *Nat Methods* 2007;4:445–453.

10. Haralick RM: Statistical and structural approaches to texture. *Proc IEEE* 1979;67:786–804.

11. Wu Y, Brodt P, Sun H, *et al.*: Insulin-like growth factor-I regulates the liver microenvironment in obese mice and promotes liver metastasis. *Cancer Res* 2010;70:57–67.

12. Manns J, Daubrawa M, Driessen S, *et al.*: Triggering of a novel intrinsic apoptosis pathway by the kinase inhibitor staurosporine: activation of caspase-9 in the absence of Apaf-1. *FASEB J* 2011;25:3250–3261.

13. Ho C-Y, Wong C-H, Li H-Y: Perturbation of the chromosomal binding of RCC1, Mad2 and survivin causes spindle assembly defects and mitotic catastrophe. *J Cell Biochem* 2008;105:835–846.

14. Iversen PW, Eastwood BJ, Sittampalam GS, Cox KL: A comparison of assay performance measures in screening assays: signal window, Z′ factor, and assay variability ratio. *J Biomol Screen* 2006;11:247–252.

15. Zhang J-H, Chung TDY, Oldenburg KR: A simple statistical parameter for use in evaluation and validation of high throughput screening assays. *J Biomol Screen* 1999;4:67–73.

16. Jones T, Kang I, Wheeler D, *et al.*: CellProfiler Analyst: data exploration and analysis software for complex image-based screens. *BMC Bioinformatics* 2008;9:482.

17. Xu JJ, Henstock PV, Dunn MC, Smith AR, Chabot JR, de Graaf D: Cellular imaging predictions of clinical drug-induced liver injury. *Toxicol Sci* 2008; 105:97–105.

18. Nagaria TS, Williams JL, Leduc C, Squire JA, Greer PA, Sangrar W: Flavopiridol synergizes with sorafenib to induce cytotoxicity and potentiate antitumorigenic activity in EGFR/HER-2 and mutant RAS/RAF breast cancer model systems. *Neoplasia* 2013;15:939–951.

19. Misra RN, Xiao HY, Kim KS, *et al.*: N-(cycloalkylamino)acyl-2-aminothiazole inhibitors of cyclin-dependent kinase 2. N-[5-[[[5-(1,1-dimethylethyl)-2-oxazolyl]methyl]thio]-2-thiazolyl]-4- piperidinecarboxamide (BMS-387032), a highly efficacious and selective antitumor agent. *J Med Chem* 2004;47:1719–1728.

20. Talekar M, Ganta S, Amiji M, *et al.*: Development of PIK-75 nanosuspension formulation with enhanced delivery efficiency and cytotoxicity for targeted anti-cancer therapy. *Int J Pharm* 2013;450:278–289.

21. Wu CP, Hsiao SH, Luo SY, *et al.*: Overexpression of human ABCB1 in cancer cells leads to reduced activity of GSK461364, a specific inhibitor of polo-like kinase 1. *Mol Pharm* 2014;11:3727–3736.

22. Ansbro MR, Shukla S, Ambudkar SV, Yuspa SH, Li L: Screening compounds with a novel high-throughput ABCB1-mediated efflux assay identifies drugs with known therapeutic targets at risk for multidrug resistance interference. *PLoS One* 2013;8:e60334.

23. Rudolph D, Steegmaier M, Hoffmann M, *et al.*: BI 6727, a Polo-like kinase inhibitor with improved pharmacokinetic profile and broad antitumor activity. *Clin Cancer Res* 2009;15:3094–3102.

24. Ho CY, Ludovici DW, Maharoof US, *et al.*: (6,7-Dimethoxy-2,4-dihydroindeno[1,2–c]pyrazol-3-yl)phenylamines: platelet-derived growth factor receptor tyrosine kinase inhibitors with broad antiproliferative activity against tumor cells. *J Med Chem* 2005;48:8163–8173.

25. Cyr L, Langler R, Lavigne C: Cell cycle arrest and apoptosis responses of human breast epithelial cells to the synthetic organosulfur compound p-methoxyphenyl p-toluenesulfonate. *Anticancer Res* 2008;28:2753–2763.

26. Chen T, Wang C, Liu Q, *et al.*: Dasatinib reverses the multidrug resistance of breast cancer MCF-7 cells to doxorubicin by downregulating P-gp expression via inhibiting the activation of ERK signaling pathway. *Cancer Biol Ther* 2015;16:106–114.

27. Yang J, Ikezoe T, Nishioka C, Furihata M, Yokoyama A: AZ960, a novel Jak2 inhibitor, induces growth arrest and apoptosis in adult T-cell leukemia cells. *Mol Cancer Ther* 2010;9:3386–3395.

Address correspondence to:
David W. Andrews, PhD
Department of Biological Sciences
Sunnybrook Research Institute
2075 Bayview Avenue
Toronto, ON M4N 3M5
Canada

E-mail: david.andrews@sri.utoronto.ca

Abbreviations Used

α-MEM	= α-minimal essential medium
BFA	= brefeldin A
DMSO	= dimethylsulfoxide
DTT	= dithiothreitol
Grp	= glucose-regulated protein
LC3	= light chain 3
mCer	= monomeric Cerulean
NAO	= nonyl acridine orange
PARP	= poly-ADP ribose polymerase
PI	= propidium iodide
SVM	= support vector machine
TG	= thapsigargin
TMRE	= tetramethylrhodamine, ethyl ester
TNFα	= tumor necrosis factor-alpha